Determinants of the Exclusion Zone in Dopaminergic Amacrine Cell Mosaics

MARY A. RAVEN,[1] STEPHEN J. EGLEN,[2] JOHN J. OHAB,[1]
AND BENJAMIN E. REESE[1]*
[1]Neuroscience Research Institute and Department of Psychology, University of California
at Santa Barbara, Santa Barbara, California 93106-5060
[2]Department of Anatomy and Neurobiology, Washington University School of Medicine,
St. Louis, Missouri 63110

ABSTRACT

A fundamental organizing feature of the retina is the presence of regularly spaced distributions of neurons, yet we have little knowledge of how this patterning emerges during development. Among these retinal mosaics, the spatial organization of the dopaminergic amacrine cells is unique: using nearest-neighbor and Vornoi domain analysis, we found that the dopaminergic amacrine cells were neither randomly distributed, nor did they achieve the regularity documented for other retinal cell types. Autocorrelation analysis revealed the presence of an exclusion zone surrounding individual dopaminergic amacrine cells and modeling studies confirmed this organization, as the mosaic could be simulated by a minimal distance spacing rule defined by a broad set of parameters. Experimental studies determined the relative contributions of tangential dispersion, fate determination, and cell death in the establishment of this exclusion zone. Clonal boundary analysis and simulations of proximity-driven movement discount tangential dispersion, while data from *bcl-2* overexpressing mice rule out feedback-inhibitory fate-deterministic accounts. Cell death, by contrast, appears to eliminate dopaminergic amacrine cells that are within close proximity, thereby establishing the exclusion zone surrounding individual cells and in turn creating their mosaic regularity. J. Comp. Neurol. 461:123–136, 2003.   © 2003 Wiley-Liss, Inc.

Indexing terms: nearest neighbor; Voronoi domain; autocorrelation; density recovery profile; tangential dispersion; fate determination; cell death; bcl-2

Many types of retinal neurons are distributed across the surface of the retina as orderly arrays, ensuring a uniform sampling of the visual field (Wässle and Reimann, 1978). The global patterning in these "retinal mosaics" is thought to be brought about by local cell–cell interactions during development that produce a minimal spacing between neighboring cells (Cook and Chalupa, 2000; Eglen and Willshaw, 2002; Reese and Galli-Resta, 2002). Such minimal spacing constraints between neighboring cells may be established during development by lateral inhibitory events controlling the fate of newborn neuroblasts (Reh and Tully, 1986; Wikler and Rakic, 1994; McCabe et al., 1999), or by the selective death of cells (Jeyarasasingam et al., 1998). Still other studies have shown that certain cell types — those very types forming regular retinal mosaics — disperse tangentially upon the retina at the time of their morphological differentiation (Reese et al., 1995, 1999) and modeling studies have shown how such short-distance dispersion propelled by mutual cell repulsion can transform an irregular distribution of neurons into a more

orderly one (Eglen et al., 2000, 2003). Any of these three biological mechanisms could in principle establish the periodicity found in a retinal mosaic. Here we examine the relative contributions of all three to the mosaic of dopaminergic amacrine (DA) cells.

The DA cells are one of the most sparsely distributed types of retinal neuron. This cell class plays a neuromodu-

latory role associated with light adaptation and the transition between scotopic and photopic vision, rather than participating in the transmission of spatial information associated with the pattern of photoreceptor activation (Xin and Bloomfield, 1999; Weiler et al., 2000; Puopolo et al., 2001), and might not be expected to be regularly distributed. Their distribution in the mouse retina has been variously described as "randomly distributed" (Versaux-Botteri et al., 1984), "irregular" (Gustincich et al., 1997), or "regularly ordered" (Wulle and Schnitzer, 1989), but how this was determined in each of those studies was not clearly defined. We have reexamined the issue of mosaic regularity for the population of DA cells, using the classic nearest-neighbor (NN) analysis as well as Voronoi domain (VD) analysis, and have determined whether the DA cells exhibit minimal spacing constraints, evidenced by autocorrelation analysis and the density recovery profile (DRP) derived from it. In each case we compared the real data to random simulations of comparable density, constrained by the physical size of the dopaminergic cell somas. We additionally defined the spacing rules that best simulate the real distribution of the DA cells.

To identify potential biological mechanisms that underlie the minimal distance spacing constraints in the population of DA cells, we first asked whether tangential dispersion is sufficient for creating the order found in this population using clonal boundary analysis (Reese and Tan, 1998). We identified the dispersion distances of these cells and subsequently asked whether random simulations could be modulated by these dispersion statistics to generate the patterning characteristic of this population. Second, we asked whether fate determination events or selective cell death might underlie the exclusion zones by examining *bcl-2* overexpressing mice, in which the patterning and minimal distance spacing constraints were determined in retinas containing a 10-fold increase in their DA cell population (Strettoi and Volpini, 2002). While tangential dispersion was found to be insufficient, and lateral inhibition does not prohibit neighboring cells from adopting the dopaminergic fate, selective neuronal death eliminates DA cells in close proximity to one another, thereby creating the exclusion zone and establishing the mosaic regularity of the DA cells.

MATERIALS AND METHODS

C57BL/6 mice obtained from Charles River Labs (Cambridge, MA) were bred and litters were reared to 3 weeks of age. Mice were deeply anesthetized with 120 mg/kg of sodium pentobarbital (i.p.) and then perfused intracardially with 5 ml of 0.9% saline followed by 20 ml of 4% paraformaldehyde in sodium phosphate buffer (pH 7.2, 20°C). Retinas were dissected from the eyecups and prepared as wholemounts, being subsequently processed for immunohistochemistry using a mouse monoclonal antibody to tyrosine hydroxylase (TH; 1:10,000; Sigma, St. Louis, MO) and standard streptavidin-biotin-horseradish peroxidase detection procedures (Vectastain Elite ABC kit; Vector, Burlingame, CA). Whole eyecups were also cryosectioned at 16 μm and immunostained and adjacent negative control sections were also prepared. A fuller account of these routine procedures is provided elsewhere (Reese et al., 1999).

Sixteen well-labeled retinas were examined as retinal wholemounts, from which a subset of seven permitted at least three 1,100 μm × 1,100 μm fields to be sampled from different retinal quadrants (e.g., Fig. 1c, right). The area of each retina was determined (average and SD = 11.14 ± 1.13 mm²) and all retinas were subsequently scaled to the average size of those seven retinas to control for slight differences in retinal size that would otherwise increase the variance in our spatial analyses. The X-Y coordinates of the positions of each TH-immunoreactive cell were determined using a video camera and Bioquant Nova Prime software (R&M Biometrics, Nashville, TN). The areas of 100 adjacent TH-immunoreactive cells were also determined from six of the seven retinas using the Bioquant software. These 600 somal areas were then converted to diameters for circular profiles of equivalent area, from which a population mean and SD was defined, and subsequently used to constrain our random simulations of equivalent density.

For each sampled retina the X-Y positional data were used in one of two manners: First, we identified at least three wings in each wholemount within which we could position a square field 1.21 mm². This yielded a total of 22 sampled fields that were used for NN and VD analyses (four fields from one retina, and three from each of the other six retinas). A minimum of 30% of each retinal area was therefore sampled. Second, we took the entire distribution of X-Y positions in each retina and conducted autocorrelation analyses upon them.

Nearest-neighbor and Voronoi domain analyses

For each sampled field we determined the NN distances and the VD areas for each cell in the field, excluding those cells whose VDs intersected the boundary, using software designed for this purpose. For each sampled field we also generated 10 random simulations of equivalent density, in which the simulation was constrained by the distribution of TH-immunoreactive soma diameters. Specifically, as each additional cell was placed in the field, the prohibited region around previously placed cells was drawn from a Gaussian distribution having the mean and standard deviation of the real distribution of soma diameters. The distributions of NN distances and VD areas were then compared with the average distributions for those random simulations. Because the density of TH-immunoreactive somas is so low, we did not want to place excessive emphasis upon spuriously regular fields. At the same time, we felt that focusing upon only those fields with high density would not adequately convey a sense of the uniformity (or lack thereof) with which the TH-immunoreactive cells actually tile the retina. Consequently, we pursued a conservative strategy of sampling from each retina where we could obtain these large fields, simultaneously generating 10 random simulations of identical density for each field. We then pooled those populations of NN distances and VD areas derived from the sampled fields in each animal to generate an average frequency distribution and compared this to the data from the random simulations. While it should be obvious that the very largest NN distances or VD areas would be relatively undersampled as they approach the dimensions of the sampled field size (and will be more frequent in the least dense samples), our random simulations of equivalent density will be similarly susceptible to this sampling bias. We also calculated the regularity indexes (RIs) derived from the NN distributions and from the VD distri-
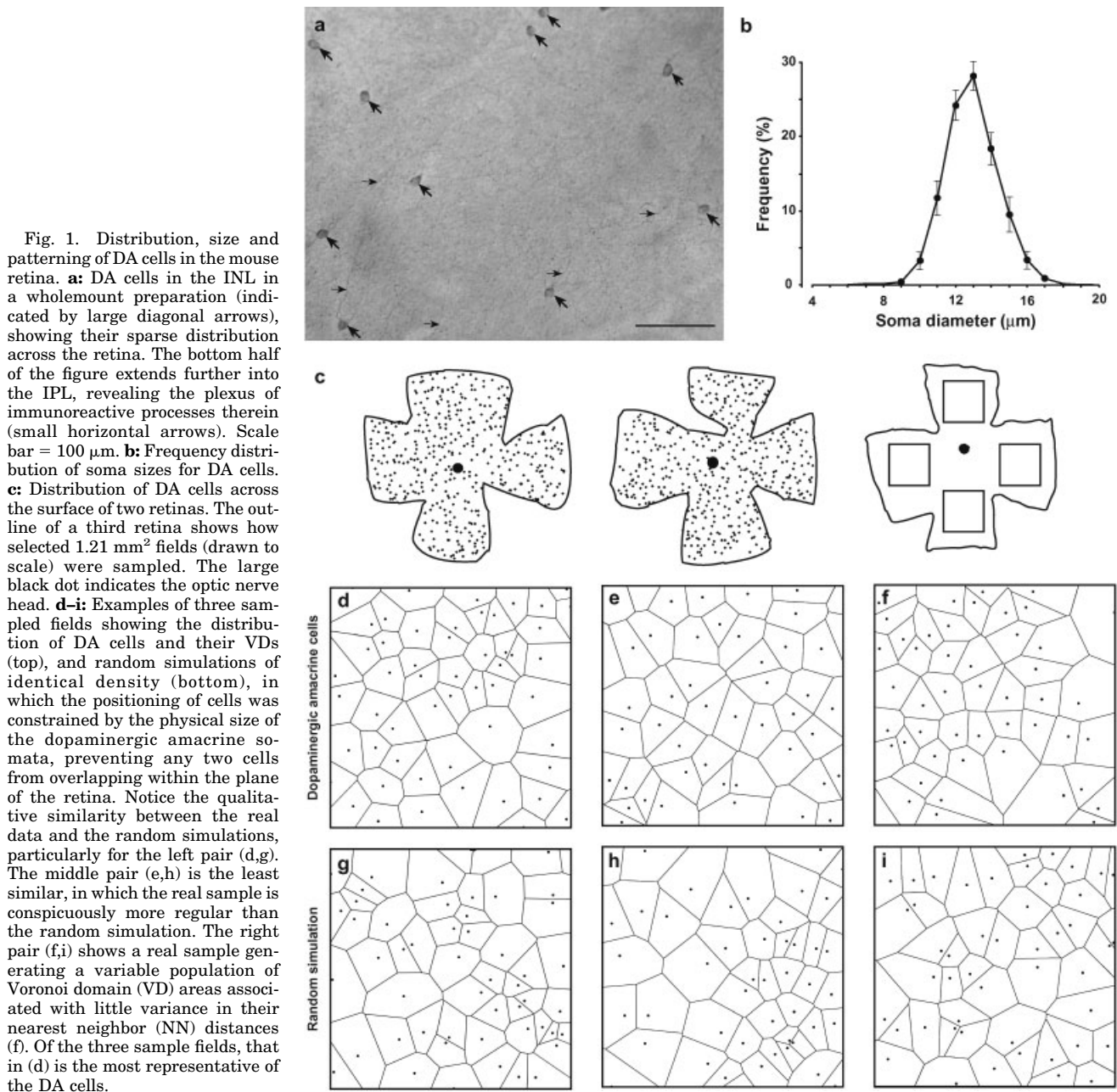
Fig. 1. Distribution, size and patterning of DA cells in the mouse retina. **a:** DA cells in the INL in a wholemount preparation (indicated by large diagonal arrows), showing their sparse distribution across the retina. The bottom half of the figure extends further into the IPL, revealing the plexus of immunoreactive processes therein (small horizontal arrows). Scale bar = 100 μm. **b:** Frequency distribution of soma sizes for DA cells. **c:** Distribution of DA cells across the surface of two retinas. The outline of a third retina shows how selected 1.21 mm² fields (drawn to scale) were sampled. The large black dot indicates the optic nerve head. **d–i:** Examples of three sampled fields showing the distribution of DA cells and their VDs (top), and random simulations of identical density (bottom), in which the positioning of cells was constrained by the physical size of the dopaminergic amacrine somata, preventing any two cells from overlapping within the plane of the retina. Notice the qualitative similarity between the real data and the random simulations, particularly for the left pair (d,g). The middle pair (e,h) is the least similar, in which the real sample is conspicuously more regular than the random simulation. The right pair (f,i) shows a real sample generating a variable population of Voronoi domain (VD) areas associated with little variance in their nearest neighbor (NN) distances (f. Of the three sample fields, that in (d) is the most representative of the DA cells.

butions for each sampled field, being the average NN distance or VD area divided by the SD, and compared each of those with the indexes from their 10 respective random simulations. The NN distances or VD areas for cells whose VD intersected the boundary were always excluded.

Autocorrelation and density recovery profile analyses

The autocorrelogram for the entire distribution of TH-immunoreactive cells was prepared for each of the seven retinas using software designed for this purpose. In brief, this program positions a cell at the origin of the autocorrelogram and then plots the position of every other cell relative to the origin. This is then repeated for every cell in the retina, thereby achieving a plot describing the relative density of TH-immunoreactive cells at increasing distances from each cell (Rodieck, 1991; Cook, 1996). The resultant autocorrelograms, derived from larger samples than those that could be generated from the 1.21 mm² sample fields, permits a clearer determination of whether local spacing constraints are present in this population of cells. We truncated these autocorrelograms at 500 μm from the origin. From this, one can generate the DRP, which is a graphical depiction of density in the autocorrelogram as a function of eccentricity from the origin in 20 μm increments, generated by determining the number of cells in each annulus of the autocorrelogram divided by the area of each annulus (Rodieck, 1991; Cook, 1996).

Such autocorrelograms and DRPs display a central region of reduced density. Some of this will be due to the physical size of the cell, assuming no two cells can occupy the same area on the retinal surface. Consequently, we generated 70 random simulations matched in average density within a square field of equivalent area and constrained by the soma diameters derived from the real data to estimate the contribution of soma size alone upon the shape of the DRP.

Modeling the exclusion zone

Simulations of the exclusion zone (or the "minimal distance spacing rule" defining it—the d_{min} model; Galli-Resta et al., 1999) were generated using similar procedures for producing the random simulations described above but using values of d_{min} greater than the soma diameter. Values less than 12 µm generated for any d_{min} simulation were prohibited in order to preserve the constraint imposed by soma diameter that no two cells could overlap. To test whether a given d_{min} rule fit a particular field, we compared the real data to the model on six different cumulative distribution functions that describe different features of the geometry of a mosaic: the NN distance; the distance to the nearest grid point for each cell (Diggle, 1983); Ripley's L function, being the scaled number of cells within a given distance of each cell (Ripley, 1976); the VD area; the internal angles within each Voronoi polygon (Shapiro et al., 1985); and the Delauney segment lengths, being all of the near-neighbor distances defined by Voronoi boundaries (Ammermüller et al., 1993). To account for possible boundary effects, two different techniques were used when calculating these measures. For the L function, a correction factor (Diggle, 1983) was used for cells near the border of the sample. For the Voronoi-based distributions, measures from cells whose VDs intersected the field boundary were not included. By using six complementary measures, we were able to compare the effectiveness of the d_{min} simulations in replicating multiple properties of the mosaics.

For any d_{min} rule, we generated 99 simulations and plotted the cumulative distribution of the lower, mean, and upper bounds of the simulations along with the experimental data. The d_{min} parameters of any given model were judged to be a good fit if the real data fell within the bounds of the simulations. A goodness-of-fit statistic based on a ranking procedure was also used, measuring the integrated distance (eq. 4.5 from Diggle, 1979) between each distribution and the mean of the 99 other distributions. In this test statistic, the lower the rank (P), the better the fit between the model and the experimental data. P-values ≥ 0.95 are considered significantly different. The four densest sample fields with a minimum of 30 VDs were simulated in this manner, in which the d_{min} parameters were systematically varied (mean diameter = from 30–150 µm, and SD = 20–60 µm, both at 10-µm intervals).

Determining dispersion distances in X-inactivation transgenic mice

Only a minority (~20%) of DA cells have been reported to disperse tangentially (Reese et al., 1999). To determine the maximal distances dispersed by these DA cells, we measured the dispersion distance of such double-labeled (transgene-expressing cells—blue, that are also dopaminergic—brown) in wholemounts from three different X-inactivation transgenic retinas that had been pro-

cessed for both β-galactosidase histochemistry and for tyrosine hydroxylase immunocytochemistry (Reese et al., 1999). Each retinal wholemount was scanned at high magnification until a minimum of 80 double-labeled cells had been encountered. Each cell was classified as residing in either a blue column or in a white column by focusing through the full retinal thickness and, for those cells residing in white columns, their distance to the edge of the nearest blue column was determined. Since half of every retinal cell type is blue in these X-inactivation mosaic mice, ~200 DA cells will be blue. Consequently, about 40% of the retinal surface must be sampled from each animal to encounter at least 80 blue DA cells. For comparison, we also measured the dispersion distances for horizontal cells from three different X-inactivation transgenic retinas that had been processed for both β-galactosidase histochemistry and for calbindin immunocytochemistry (Reese et al., 1995). The dispersion distance of a cell is the minimum distance of that cell to the edge of the nearest blue — transgene-expressing — column. This is a necessarily conservative estimate, as described in detail elsewhere (Reese and Tan, 1998). Chimeric mice containing a minority of transgenic clones were also examined (Reese et al., 1999).

Modeling the effect of tangential dispersion

Ten random simulations, matched in density to the average for the DA cell mosaics (i.e., 48 cells in a field of 1.21 mm²) were generated. These simulations were then modified by the dispersion distance data generated from the analysis of the X-inactivation *lacZ* transgenic mice described above. Specifically, 20% of the population was selected for dispersion and these cells were dispersed at either 1) the largest dispersion distance observed, being 20 µm; 2) an intermediate dispersion distance, 10 µm; or 3) at the relative frequencies identified for the DA cells (that is, at some variable distance from 5–20 µm, with frequencies matching the real data described in Fig. 4d). As our goal was to determine whether tangential dispersion might be sufficient to transform random mosaics into mosaics with the regularity characteristic of DA cells, we selected for dispersion the 20% of the cells having the smallest NN distances, moving each cell away from its neighbor along a vector running through the pair of cells. Only those cells with VDs free of the field boundary were eligible for movement, so that if a field of 48 cells had only 25 cells yielding complete VDs, then only 20% of this population (i.e., five cells) were moved. The RIs of the new distributions were then compared with the initial distributions before movement.

Measuring mosaic regularity and the size of the exclusion zone in *bcl-2* overexpressing mice

The digital images of 32 fields taken from each of four different *bcl-2* overexpressing retinas that had been immunostained for tyrosine hydroxylase were made available to us by Dr. Enrica Strettoi (Strettoi and Volpini, 2002). From these fields we selected the densest field from the center and the periphery along each of the four primary axes across each retina for further examination, in which we identified the NN distances and VDs of each cell, excluding those whose VDs intersected the boundary of the field. As field size in that original study (Strettoi and Volpini, 2002) was small relative to the above fields in wildtype retina, being only 312.5 µm × 312.5 µm (about

one-twelfth of the size of those fields), this reduced the total number of cells yielding NN distances within a field, despite their 10-fold increase in density in these retinas. Only seven of those 32 examined fields generated 10 or more NN distances, and these were all derived from two of the four original animals. We therefore concentrated our analysis on those seven fields, computing their RIs. For each field, 10 random simulations matched for field size and density were generated, constrained by soma diameter as above. For each of these seven real and 70 random simulations, NN and VD analyses were conducted from which their RIs were calculated. Autocorrelograms were also generated from each of those fields, from which the average DRP was constructed for these two populations. Because of the small size of the fields these autocorrelograms examined only a 50 μm radius surrounding each cell, in 10 μm increments, and those cells within 50 μm of the border were excluded.

RESULTS
Dopaminergic amacrine cell density and distribution

The TH-immunoreactive amacrine cells identified in wholemounts (Fig. 1a) and in retinal sections confirm the general descriptions provided by others for the mouse retina (Versaux-Botteri et al., 1984; Wulle and Schnitzer, 1989; Gustincich et al., 1997). These cells are situated almost entirely within the inner nuclear layer (INL) at the boundary with the inner plexiform layer (IPL), with less than 1% being displaced into the ganglion cell layer (GCL), as in the rat retina (Martin-Martinelli et al., 1994), and to be contrasted with the carnivore retina in which nearly a third are found in the GCL (Peichl, 1991). They have relatively large somas ranging from 9–16 μm in diameter (Fig. 1b), the average being 11.43 μm (±1.45 μm; all values in the text are for mean and SD). Each gives rise to a diffuse arbor of dendritic and axonal processes that is TH-immunoreactive, situated in S_1 of the IPL (small arrows in Fig. 1a), with branches occasionally extending into the OPL (Versaux-Botteri et al., 1984; Wulle and Schnitzer, 1989; Gustincich et al., 1997). These TH-immunoreactive cells are believed to be the DA cells (Gustincich et al., 1997). A second population of smaller TH-immunoreactive cells with pear-shaped somata has also been described, which in our material are very rarely encountered and are only faintly immunopositive. These are regarded as being catecholaminergic cells that do not use dopamine as their neurotransmitter, now documented in multiple species of mammals (Mariani and Hokoc, 1988; Nguyen-Legros, 1988; Tauchi et al., 1990; Gustincich et al., 1997), and are not considered further.

The mouse retina has on average 400 DA cells. These cells are distributed across the retinal surface, showing no obvious variation with retinal eccentricity nor quadrant (Fig. 1c), aside from a reduced density near the optic nerve head in some specimens. The average cell density over the entire retina was 35.7 ± 3.58 cells per mm². By contrast, the average density for our sampled fields was slightly higher, being 39.3 ± 6.76 cells per mm². These densities are all higher than those reported by others (e.g., 26–32 cells per mm²; Versaux-Botteri et al., 1984; Wulle and Schnitzer, 1989; Gustincich et al., 1997; Strettoi and Volpini, 2002), because the retina has not expanded to its mature size by 3 weeks of age.

Mosaic regularity of dopaminergic amacrine cells

The spatial patterning of DA cells for three sampled fields is shown in Figure 1d–f (containing 44, 40, and 40 cells per mm², respectively), with their VDs indicated. Beneath each field is one of 10 random simulations (Fig. 1g–i) that had been generated at a density matched to the real sample above and constrained by soma size, looking not unlike the real distributions. What is conspicuous about these mosaics, relative to the distributions of cholinergic amacrine cells or horizontal cells in the mouse retina (Galli-Resta et al., 1997; Raven and Reese, 2002), is just how irregular they appear, made obvious by the variability in their VDs here, particularly in Figure 1d. Yet measurements of the VD areas from the sample fields reveal that their distribution is not identical to that derived from the random simulations, with fewer of the smallest VD areas being present in the real data (Fig. 2a; $P < 0.001$, Kolmogorov-Smirnov two-sample test). A comparison of NN distances reveals this same qualitative difference (Fig. 2b): the distribution of NN distances for the real data averages 92.7 μm, while that for the random simulations averages 74.5 μm, and the distributions differ for all NN distances less than 160 μm ($P < 0.001$, Kolmogorov-Smirnov test).

The NN distributions show that DA cells are almost never found within 20 μm of one another, and that at all distances less than 80 μm they occur less often than one would predict from a random distribution of cells (Fig. 2b). Yet the distribution of real NN distances is not a Gaussian distribution typical of regular retinal mosaics, for it contains a tail at longer NN distances (>160 μm) that is similar to that exhibited by the random simulations (Fig. 2b). Likewise, the distribution of VDs for both the real and random data indicate that both populations have an identical (if rather small) number of very large domain areas (Fig. 2a), also evidenced in Figure 1d,f. These data together imply that the DA cells are more regular than are the random simulations, but not tremendously so. This is borne out by a comparison of the RIs derived from the NN distributions for these 22 individual sampled fields, averaging 3.06 ± 0.91. The range of regularity indices for these samples was substantial, extending from 1.95–5.65, yet this variation did not correlate with cell density, unlike the rod photoreceptors in the ground squirrel's retina (Galli-Resta et al., 1999). While every field generated larger RIs than was found for the average of 10 random simulations matched to the density of each sampled field, in a few cases the index was only marginally better. Those averaged random simulations, close to the theoretical limit of 1.91 for a random population (Cook, 1996), do not give a sense of the variability within each set of 10 density-matched simulations. To appreciate just how often spuriously high RIs are obtained with such low numbers of cells in a field, Figure 2c plots the range of regularity indices for the real data (left), compared directly with the range of regularity indices for the random simulations (middle) matching the field with 1) the smallest RI, 2) the largest RI, 3) the sparsest density, and 4) the greatest density. For comparison, the range of RIs for a population of cells known to be distributed as a regular mosaic, the horizontal cells, is also shown (right; from Raven and Reese, 2002). These results show that while many of the regularity indices surpass the range expected
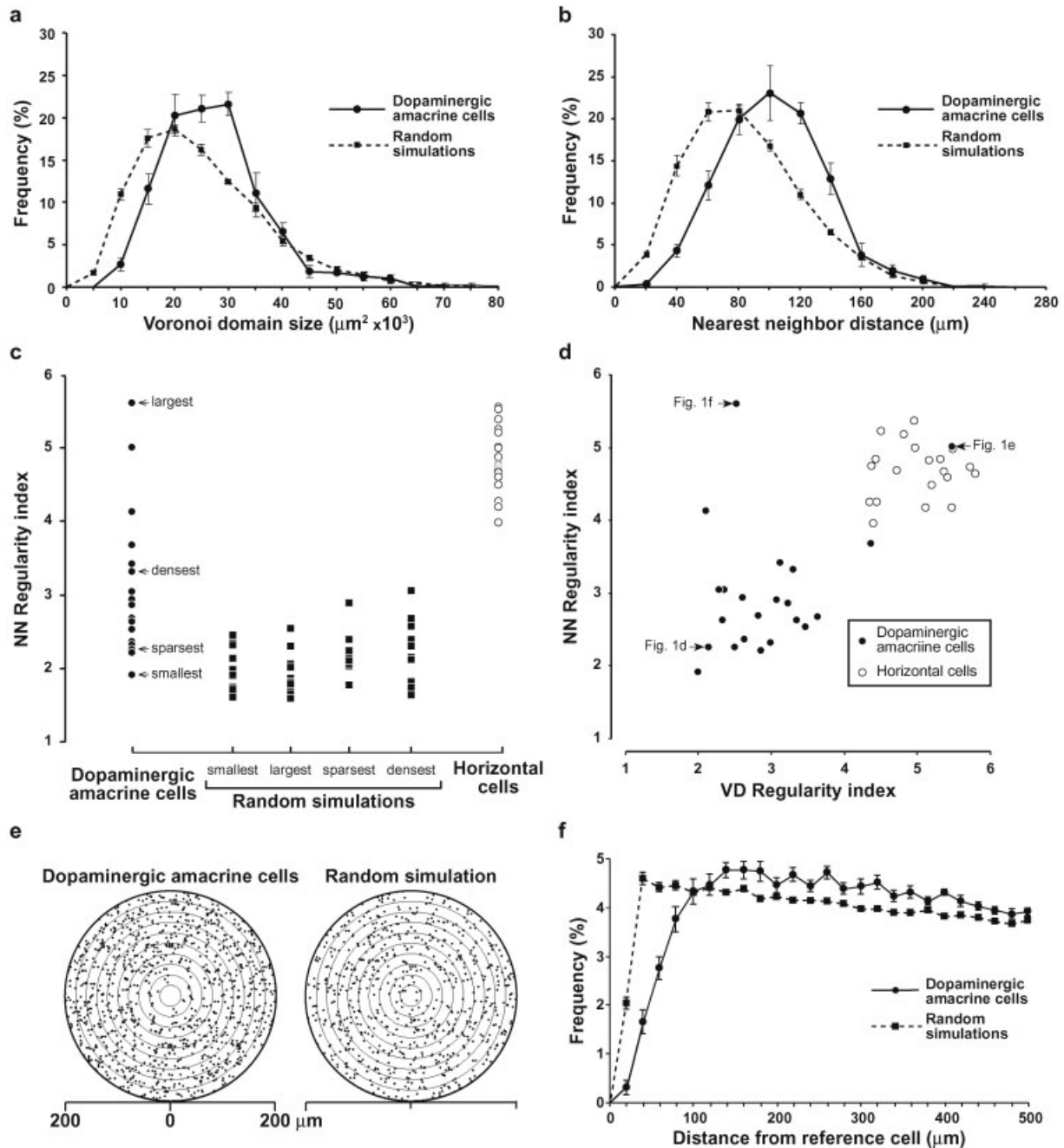
Fig. 2. Regularity and spacing of DA cells. **a:** Distribution of VD areas for the population of DA cells (solid line). Each point indicates the mean and standard error for that bin, averaged across fields. For comparison, the distribution of VD areas for all of the cells within the random simulations is shown (broken line). **b:** Distribution of NN distances for the DA cells (solid line) and random simulations (broken line). **c:** NN regularity indexes (RI) for the 22 sampled fields of DA cells (filled circles), from the 10 random simulations associated with four of the real fields (filled squares) and from 20 sampled fields of horizontal cells (open circles). **d:** RIs derived from the NN analysis as a function of their RIs derived from the VD analysis, for both DA cells (filled circles) and horizontal cells (open circles). The RIs are positively correlated and the two populations of cells cluster at relatively low or high indices, respectively. Notice, however, four exceptions among the DA cell samples — two overlap the cluster of horizontal cells (e.g., Fig. 1e), while two others have high NN RIs that overlap those of the horizontal cells but low VD RIs (e.g., Fig. 1f). **e:** Central 200 μm from an autocorrelogram derived from the spatial distribution of DA cells from one entire retina (left). Autocorrelogram derived from a random simulation constrained by the physical size of the DA cells (right), for comparison. Annuli are spaced 20 μm apart. **f:** Average density recovery profile (DRP) showing the relative density of DA cells at increasing eccentricities from each DA cell (solid line). Means and standard errors are plotted, derived from the DRPs prepared from each animal. The DRP derived from random simulations is shown for comparison (broken line), indicating that an exclusion zone surrounding individual DA cells is conspicuously greater in size than would be predicted from soma size alone.

from random distributions of cells, other fields do not differ from these random distributions. A few of the fields overlap with the range of the horizontal cells, but these are clearly not representative.

Figure 2d plots the NN RI as a function of the VD RI, for both the DA cells and the horizontal cells. From this, it is clear that these two measures of regularity extract related information about the spatial arrangement of the mosaics, even if they are not perfectly correlated. The mosaics fall mostly into two clusters, showing on the whole that the horizontal cells are more regular than the DA cells. However, we also see that two of the DA cell mosaics have regularity indices overlapping the cluster associated with the horizontal cell mosaics (e.g., Fig. 1e). Yet another two mosaics have high NN RIs compared to their VD RIs (e.g., Fig. 1f). This comparison in Figure 2d, then, shows that these four fields are clearly atypical; the other 18 fields have an average NN RI around 2.7. While one may conclude from either the pooled data in Figure 2a,b or from these regularity indices in Figure 2c,d that the real distribution of DA cells is on average more regular than a random simulation, it certainly does not approximate the consistently high regularity characteristic of other retinal mosaics like the horizontal cells.

Autocorrelation analysis reveals exclusion zones surrounding dopaminergic amacrine cells

The comparison of NN distances in Figure 2b indicates that DA cells are rarely closer to one another than 20 μm, whereas the average soma diameter is only 11.43 μm and random simulations generate such short distance neighbors with greater frequency. To make apparent the presence of "exclusion zones," regions surrounding each cell within which other cells of like-type are less frequently encountered, autocorrelation analysis of the entire retinal distribution of DA cells was conducted. Figure 2e (left) shows the autocorrelogram for one such retina. This figure plots the relative density of DA cells from each cell at increasing eccentricities from that cell, revealing that DA cells are never found within 20 μm of a cell in this retina. Further, their density appears to be lower in the next couple of annuli than elsewhere in the autocorrelogram. One can convert these data into graphical form by computing the DRP for each retina, and then plotting the mean and standard error for each bin, averaged across the seven retinas (solid line in Fig. 2f). Such an average DRP confirms that the density is relatively lower within a region surrounding individual cells out to about 100 μm. This region of reduced density is, of course, far greater than the exclusion zone imposed by the physical size of the soma, derived from autocorrelograms of random fields (Fig. 2e, right, and broken line in Fig. 2f). The presence of such a large exclusion zone surrounding individual DA cells may be sufficient to reduce the variability of potential NN distances and VD areas, bestowing a modicum of regularity upon an otherwise random distribution.

Simulating dopaminergic amacrine cell mosaics using minimal distance spacing rules

We have tried to simulate the DA cell mosaic by generating distributions of cells at identical density to those in the sampled fields in which the only constraint upon cel-

lular positioning is that no two cells can be closer to one another than some average distance, with some variance associated with that distance (Galli-Resta et al., 1997, 1999; Eglen et al., 2003). To test these minimal distance spacing rules (or "d_{min}" rules), we generated 99 simulations using these parameters, matched in density to a given field, and then compared the real data from that field to those 99 simulations on each of six different measures associated with the geometrical properties of the mosaic. We asked whether the real data fell within the 95% confidence limits derived from those 99 simulations for each of those six different measures, for every possible combination of simulated diameter × SD parameters, and sought to identify the range of d_{min} parameters that could simulate multiple fields. We focused on the four densest fields (derived from three different animals), as sparser fields proved to be fitted by an increasingly broad combination of possible d_{min} parameters. These four fields had NN RIs of 2.4, 2.7, 2.9 and 3.4 (being fields a, c, b, and d, respectively).

Figure 3a shows the performance of one set of d_{min} parameters (having a mean of 70 μm and an SD of 50 μm) in simulating the real data from one field (field b, with an NN RI of 2.9) for six different measures of the geometry of the mosaic, in which the model fits the data (i.e., $P < 0.95$) for all six distributions. By exploring a range of parameters of the d_{min} rule, we found many that could produce acceptable fits. For example, three out of the four fields were fit using a d_{min} of 40 ± 20 μm on all six measures. For the fourth sample (field d, with an NN RI of 3.4), this d_{min} rule could not fit the experimental data for the NN distribution and even the fit at 70 ± 50 μm was marginal ($P = 0.93$). Instead, we found progressively better fits for this field using much larger d_{min} means, although these values rarely fit all three other fields for all six distributions. Only the d_{min} rules of 70 ± 50 μm, 80 ± 60 μm, and 90 ± 60 μm were found to fit all four fields on all six of the measures.

In general, we found that many d_{min} values would fit all six different spatial distributions for a given sample. Out of the six measures, the NN distribution was generally the hardest to fit; if we obtained an acceptable fit for the NN distribution, we usually found an acceptable fit for the other five distributions. The range of P-values associated with the fit of the four sample fields to each of the d_{min} parameters, for the NN distribution, is shown in Figure 3c, while that for the VD distribution is shown in Figure 3d. Solid black regions in the figures indicate territory in the d_{min} parameter space where the goodness-of-fit is poor ($P \geq 0.95$) for all four fields, while whiter regions show fits associated with progressively lower P-values. A comparison of these two figures shows that the NN distribution is indeed the harder of the two to simulate using such d_{min} rules. Nevertheless, Figure 3c reveals the breadth of d_{min} parameters by which the NN distribution for three of the four fields can be simulated. The fact that the fields can be fitted by multiple parameters suggests that there is only a very loose regulation of proximity between cells, perhaps to be expected given the shallow border of the well in the DRP (Fig. 2f).

A consideration of the number of cells that were rejected during the creation of a simulated d_{min} mosaic conveys a sense of the frequency with which these cells infringe upon one another's exclusion zones. For example, for the 99 simulations used in Figure 3a (d_{min} parameters = 70 ±
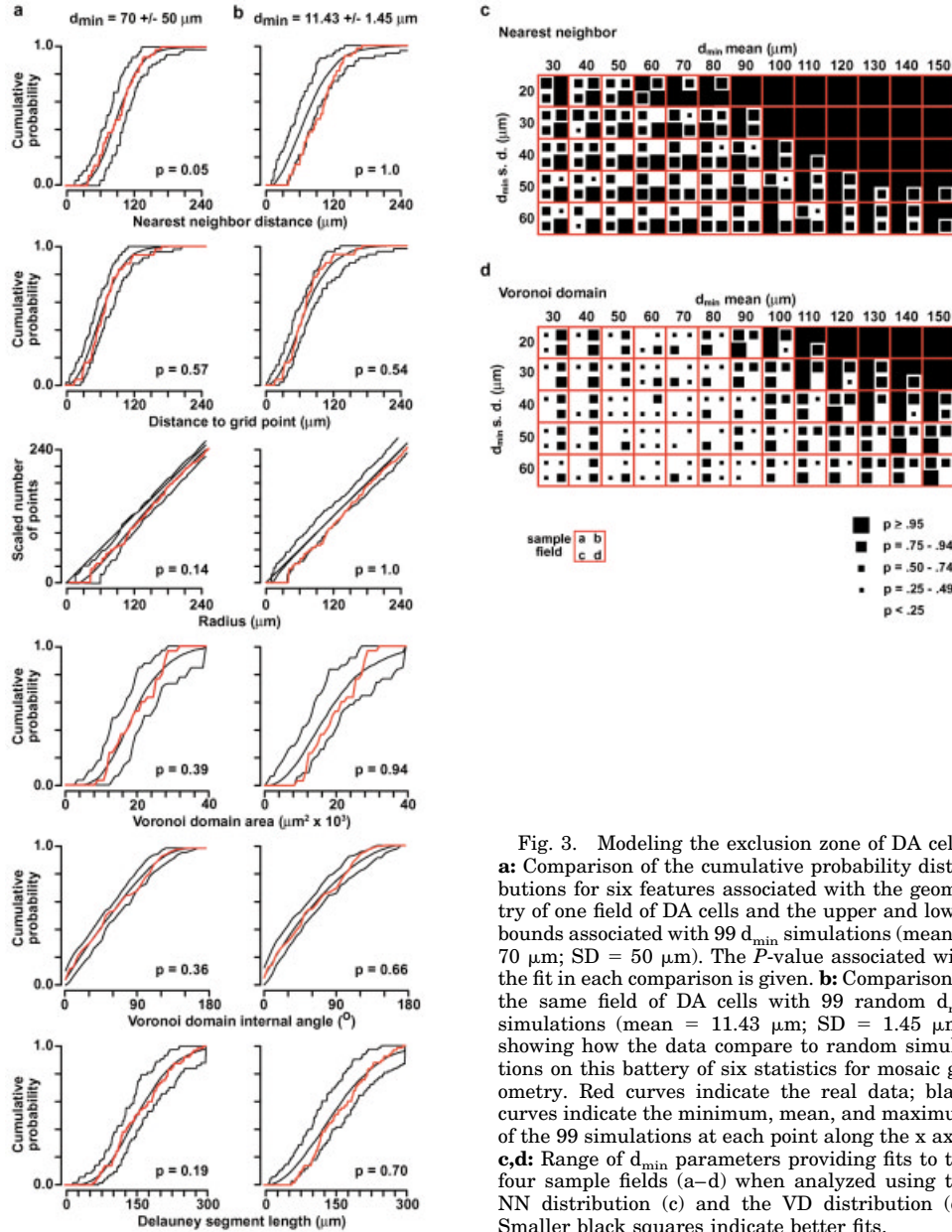
Fig. 3. Modeling the exclusion zone of DA cells. **a:** Comparison of the cumulative probability distributions for six features associated with the geometry of one field of DA cells and the upper and lower bounds associated with 99 d_{min} simulations (mean = 70 μm; SD = 50 μm). The *P*-value associated with the fit in each comparison is given. **b:** Comparison of the same field of DA cells with 99 random d_{min} simulations (mean = 11.43 μm; SD = 1.45 μm), showing how the data compare to random simulations on this battery of six statistics for mosaic geometry. Red curves indicate the real data; black curves indicate the minimum, mean, and maximum of the 99 simulations at each point along the x axis. **c,d:** Range of d_{min} parameters providing fits to the four sample fields (a–d) when analyzed using the NN distribution (c) and the VD distribution (d). Smaller black squares indicate better fits.

50 μm), each simulated d_{min} mosaic rejected 38 (±9) cells because they fell within another cell's exclusion zone. This field had only 55 cells, indicating that around 69% of them had to be replaced. To put this number of "rejects" into perspective, to simulate a mosaic of 55 cells with an RI of around 5.1 (by using a d_{min} of 100 ± 20 μm in an area 1.21 mm²), 96 (±21) cells were rejected; that is, for every cell in this simulated mosaic, nearly two cells had been rejected because they were positioned within another's exclusion zone. On the other hand, if the d_{min} is set to approximate the effect of soma size alone (i.e., 11.43 ± 1.45 μm), then simulating a field of the same size containing 55 cells yields a rejection rate of only 0.52 (±0.73). This indicates that the soma size constraint was hardly ever imposed, suggesting the points are truly random. A comparison of

such a d_{min} simulation approximating the effect of soma size alone (that is, our random simulation) with the real data from field b on each of these six measures is shown in Figure 3b, revealing the poor fit of the random d_{min} simulation to the real data on two (nearly three) of the six measures. Despite their nonrandom distribution, this population of DA cells is clearly not discriminated from random simulations using the other three measures, being the distance to nearest grid points, VD angle size, or Delauney segment length. Similar results were obtained when comparing two of the other three fields (fields a and c) to this random d_{min} rule. As suggested by the *P*-values in the parameter space shown in Figure 3c,d, field d is distinct from the other three fields, being reliably different from the random d_{min} rule on five of the comparisons. Only

Fig. 4. Simulating tangential dispersion of DA cells. **a–c:** Tangentially dispersed DA cells in chimeric retinas, shown in retinal sections (a,b) and in a whole-mount (c). Transgenic DA cells (being identified by their blue and brown reaction products, respectively) are typically found in blue columns, but a minority are displaced from those blue columns (arrows in a,c), indicating their tangential dispersion during development. Dopaminergic cells that are not transgenic are typically found in white columns (arrowhead in **c**), but are also occasionally found in blue columns, indicative of their tangential dispersion (arrow in b). Scale bar = 50 μm. **d:** Dispersion distances for the minority of DA cells that have dispersed tangentially in X-inactivation transgenic retinas (n = 27). Dispersion distances conspicuously greater than these are common among the population of dispersing horizontal cells (n = 159). Distances smaller than 20 μm have been excluded for the horizontal cells. **e:** Example of a random simulation in which 20% of the nearest neighbors whose VDs did not intersect the boundary have been moved apart 20 μm. The arrows indicate the direction of the displaced cells, while the red open circles indicate the final position of the affected cells after being moved. VDs before (black lines) and after movement (red lines) of the cells are indicated. **f:** NN RIs as a function of VD RIs for the 10 different random simulations before (black filled squares) and after (open red squares) cells had moved.
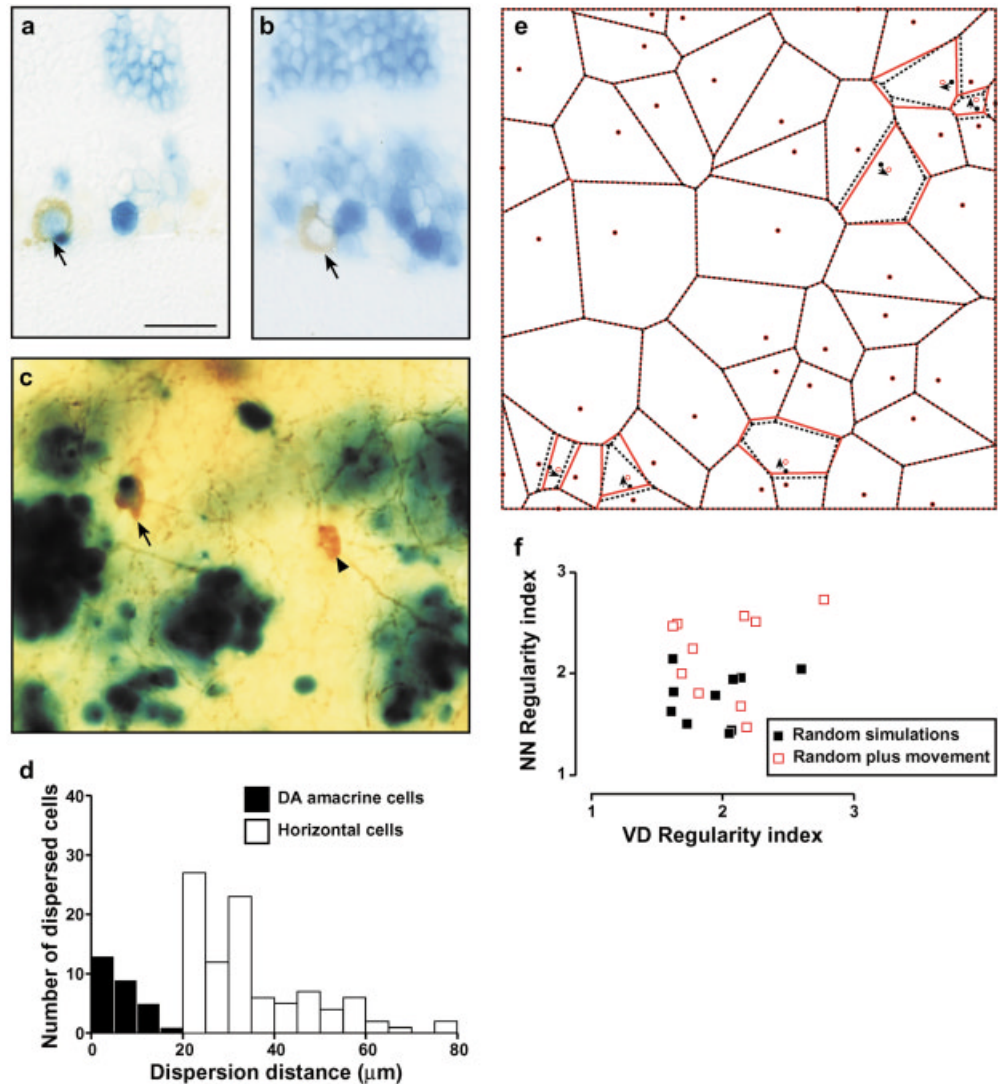
the Delauney segment length comparison failed to discriminate any of the four fields from random.

Tangential dispersion of dopaminergic amacrine cells

The exclusion zones of horizontal and cholinergic amacrine cells have been suggested to reflect the tangential dispersion of their cells during early development, as those cells interact with like-type cells to repel one another (Galli-Resta et al., 1997, 2002). Both of these cell types display universal tangential dispersion, meaning that all cells of these types move tangentially during development (Reese et al., 1999). DA cells, on the other hand, are largely confined to their own clonal columns, although a minority (~20%) are found outside of these columns (Reese et al., 1999), as shown here for three examples derived from chimeric mice in which a small number of transgenic progenitor cells has seeded an otherwise wildtype retina (Fig. 4a–c). The two blue DA cells in Figure 4a,c (arrows) situated in white regions of retina must have dispersed tangentially during development, as

must the white DA cell in the blue column in Figure 4b (arrow). Given the sparse distribution of DA cells, we considered the possibility that as little as 20% of the DA cell population moving tangentially might be sufficient to move close neighbors apart from one another, thereby transforming a random distribution of cells into a more regular one. We have, as a first step, measured the dispersion distances of these DA cells to compare those distances to the size of the exclusion zone suggested by the above DRP and d_{min} modeling studies.

Figure 4d shows the dispersion distances for 28 dispersing DA cells sampled from three X-inactivation transgenic retinas. Nearly all of them were positioned within 15 μm of the nearest blue column and most of them within 5 μm, indicating that they do not disperse far. As described elsewhere, because half of all retinal clones are blue and half are white in these transgenic retinas, a tangentially dispersing blue cell could move for some lengthy distance, yet end up underestimated by virtue of its residing near another blue (though clonally unrelated) column (Reese and Tan, 1998). However, large patches of transgene-

inexpressing retina occur occasionally in these retinas, and while other cell types are frequently observed within these patches by as much as 80 μm from the nearest blue column (e.g., horizontal cells in Fig. 4d), the DA cells never are. Unlike the X-inactivation transgenic retinas, chimeric retinas generated by blastocyst injection of a few transgenic embryonic stem cells have the advantage of containing small numbers of transgenic clones in wildtype retina, and so a blue dispersing cell is much more likely to end up in white retinal territory, reducing the likelihood that its dispersion distance will be underestimated (Reese et al., 1999). Of course, highly imbalanced chimeras will have only a few dopaminergic amacrine cells (i.e., a retina with only 1/100th of its progenitor population being transgenic should contain only four blue DA cells). Still, examination of four chimeric retinas never turned up blue DA cells that were more than 1–2 cell diameters from the nearest blue column. Whatever moves the 20% of DA cells laterally, it appears unlikely that this contributes substantially to the formation of the exclusion zone: none of these cells moves a sufficient distance upon the retina to match the range suggested by the above studies.
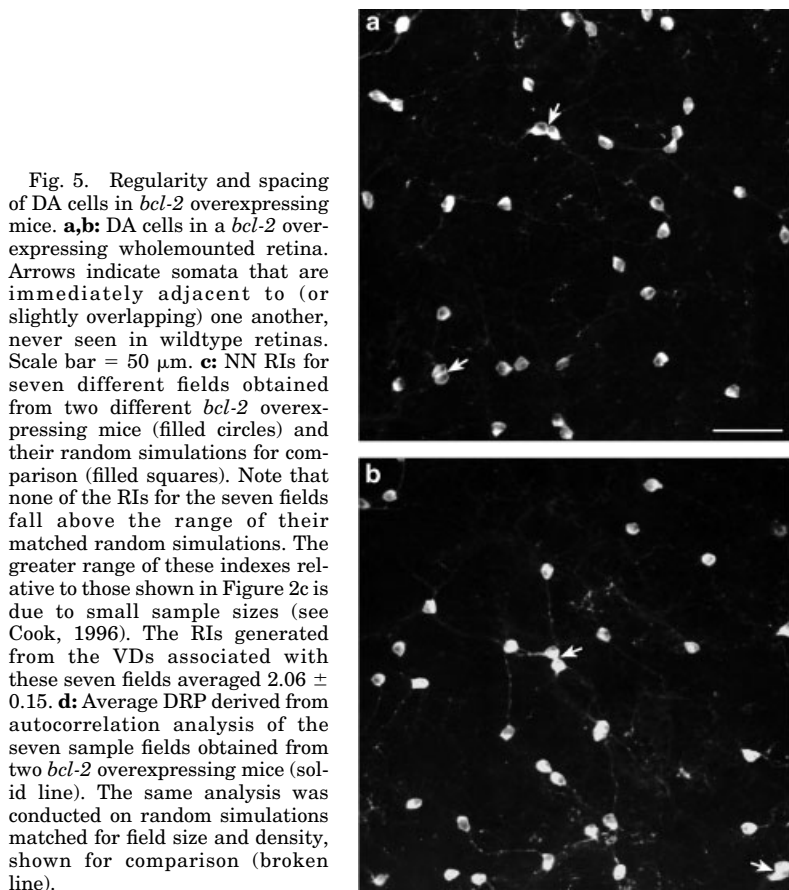
Simulating tangential dispersion

Nevertheless, to determine just how much these dispersion distances might transform a random distribution of cells into a more regular distribution, we simulated the effect of tangential dispersion by moving 20% of the closest neighbors in random simulations up to 20 μm. Ten random simulations were generated, matched in density to the average of the 22 fields. Figure 4e shows one such example, in which 20% of the cells (excluding those whose VDs intersected the boundary) were moved 20 μm. The figure makes clear that the dispersion distances are small relative to the average intercellular distance, and that the change in the geometry of the VDs is minimal. We determined the NN and VD RIs before and after moving cells, shown in Figure 4f. These data show that this tangential dispersion is effective at increasing mosaic regularity as judged by the NN RI, being an increase from 1.78 ± 0.27 to 2.23 ± 0.45. Yet this tangential dispersion does not raise regularity to levels comparable to the real distribution of DA cells, averaging 2.71 ± 0.41 (excluding the four unrepresentative fields in Fig. 2d). As indicated above, this is not surprising given the modest size of the documented dispersion distances relative to the size of the exclusion zone derived from the above experimental analysis of the real DA cell mosaics and the d_{min} modeling studies. Furthermore, these movements hardly change the RIs derived from the VD measurements. The VD RIs of the random simulations equal 1.96 ± 0.31 and climb only slightly to 2.05 ± 0.36, whereas the real mosaics average 2.81 ± 0.49. Additional simulations were performed in which cells were moved either 10 μm (closer to the real average dispersion distance detected) or by distances matching the distribution reported in Figure 4d. In both of these cases, not surprisingly, RIs were lower than in the condition reported in Figure 4f. Since 20 μm is an overestimate of average dispersion distance, we believe that the data in Figure 4f provide an upper bound on the RIs that can be achieved by tangential dispersion. The present analysis suggests that the tangential dispersion operating among DA cells does not transform a random distribution of cells into the geometry of the real dopaminergic mosaic.

Dopaminergic amacrine cell mosaics in *bcl-2* overexpressing mice

Transgenic mice overexpressing the antiapoptotic gene *bcl-2* have been shown to contain a 10-fold increase in the number of DA cells (Strettoi and Volpini, 2002). We examined the mosaic of DA cells from such *bcl-2* overexpressing mice to address the following issues: First, as indicated above, the low regularity indices of DA cells in wildtype mice are due to the low density of cells despite such large d_{min} values. As density increases, coverage may become more uniform, producing an increase in the RI, much as has been shown for the rod photoreceptors in ground squirrel (Galli-Resta et al., 1999). Second, a 10-fold increase in density might require a smaller value of d_{min} to accommodate this many cells. This should become apparent as a decrease in the size of the well in the DRP derived from autocorrelation analysis.

Figure 5a,b shows typical fields from a *bcl-2* overexpressing mouse retina in which the local density of DA cells is 348 cells/mm². The DA cells are not conspicuously regular, and this is borne out by an examination of their RIs, averaging 2.22 ± 0.46. Because the sampled fields were only 312.5×312.5 μm, the number of cells for which we could obtain NN distances was relatively small. Spuriously high RIs are of course increasingly likely with small samples, so we have compared the indexes for each of these fields with random simulations matched in field size and density (and constrained by soma size), shown in Figure 5c. Unlike some of the RIs for the DA cells in wildtype retinas (Fig. 2c), no *bcl-2* sample yielded an index greater than the range of RIs generated from their respective random simulations.

The fields shown in Figure 5a,b imply that DA cells in the *bcl-2* overexpressing retinas do not exhibit the exclusion zones observed in wildtype retinas (Fig. 2e and f). DA cells are frequently positioned side-by-side, something never observed in the normal retinas (compare with Fig. 1a; 2b,e). To determine whether the DA cells in the *bcl-2* overexpressing retinas still exhibit such exclusion zones characteristic of the normal retinas but perhaps with less fidelity, we generated an average DRP from the autocorrelograms of these *bcl-2* overexpressing samples and compared it with that derived from the matching random simulations (Fig. 5d). These two curves are near-identical, such that the well in the DRP for the real data can be accounted for by the effect of soma size entirely. This is to be contrasted with the data in Figure 2f, in which the DRP in the wildtype retina exhibited a well that was conspicuously larger than that generated by soma size alone. Likewise, the NN distribution (Fig. 2b) showed that DA cells are hardly ever found within 20 μm of one another, yet the present analysis shows that they occur within 20 μm as often as random simulations would yield. Indeed, there is even a suggestion that NN distances less than 10 μm occur more frequently in the *bcl-2* overexpressing retinas (Fig. 5d), due to their occasional if slight positional overlap (arrows in Fig. 5a,b), indicating that our assumption of no somal overlap on the retinal surface in the analysis of the normal mosaic was indeed a conservative one. The present results make clear that the spacing rules that are normally operational within the DA cell population are not preserved in *bcl-2* overexpressing mice. While the population of DA cells in the wildtype retina was found to cover the retina somewhat better than a random distri-

Fig. 5. Regularity and spacing of DA cells in *bcl-2* overexpressing mice. **a,b:** DA cells in a *bcl-2* overexpressing wholemounted retina. Arrows indicate somata that are immediately adjacent to (or slightly overlapping) one another, never seen in wildtype retinas. Scale bar = 50 μm. **c:** NN RIs for seven different fields obtained from two different *bcl-2* overexpressing mice (filled circles) and their random simulations for comparison (filled squares). Note that none of the RIs for the seven fields fall above the range of their matched random simulations. The greater range of these indexes relative to those shown in Figure 2c is due to small sample sizes (see Cook, 1996). The RIs generated from the VDs associated with these seven fields averaged 2.06 ± 0.15. **d:** Average DRP derived from autocorrelation analysis of the seven sample fields obtained from two *bcl-2* overexpressing mice (solid line). The same analysis was conducted on random simulations matched for field size and density, shown for comparison (broken line).

bution of cells, the population in *bcl-2* overexpressing mice tiles the retina no better than a random distribution.

DISCUSSION

The present study has shown that, despite the irregular appearance of the distribution of DA cells across the surface of the mouse's retina, it is not a random distribution. This is made apparent by the dissimilarity between the total distribution of NN distances or VD areas when compared to random simulations, by the greater RIs for the individual samples when compared with their average random simulations, and by the presence of large exclusion zones surrounding individual DA cells. The present study also shows that the distribution of DA cells is only marginally more regular than random distributions. This is revealed by the overlap in the distributions at longer NN distances and larger VDs when compared with random simulations, by low RIs that overlap those of the random simulations, and by the presence of large exclusion zones in the absence of cellular densities that approach the theoretical limit imposed by them.

We have used computer simulations to help further understand the spatial properties of these mosaics. We found that a random simulation, constrained only by preventing cell somas from overlapping, was insufficient at replicating those spatial features of the DA cell mosaic encompassed by the NN and VD statistics. As indicated above, these random simulations (using d_{min} parameters
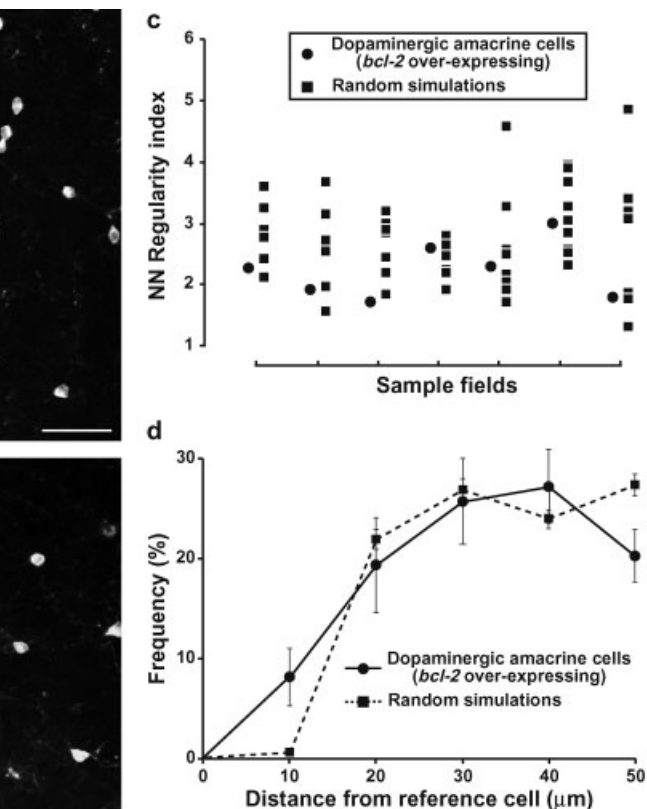
of 11.43 ± 1.45 μm) are at such low density that the frequency of rejection is on average less than one cell per field, and hence the simulations are essentially truly random ones. When, however, we enlarged the exclusion zone in these d_{min} simulations (e.g., to 70 ± 50 μm), the simulations became effective at mimicking the real mosaic of DA cells. The exact size of this exclusion zone does not appear to be critical, since multiple d_{min} parameters were found to be effective at simulating any given field. Hence, whatever mechanism is responsible for producing the exclusion zone, its efficacy varies considerably from cell to cell.

It is telling that even the d_{min} rule defining our random simulation was effective at fitting the real mosaic on three of the six spatial measures (distance to nearest grid points, VD angle, or Delauney segment length) for three of the four sample fields, betraying a degree of randomness of the DA cell mosaic that sets it apart from other regular retinal mosaics. Perhaps the most unusual feature of these cells, relative to other cell types, is that they give rise to extremely widefield dendritic arbors and extensive axonal processes that together blanket the retina within the outermost stratum, S_1, of the IPL (Kolb et al., 1981; Versaux-Botteri et al., 1984; Oyster et al., 1985; Savy et al., 1989; Wulle and Schnitzer, 1989; Dacey, 1990; Müller and Peichl, 1991). Indeed, their dendritic arbors, often asymmetrically distributed around the cell, may be oriented to compensate for the irregular distribution of their somata to ensure local uniform coverage by their pro-

cesses (Savy et al., 1989). The population of DA cells may also not tile the retina as uniformly as other retinal neurons because dopamine plays a neuromodulatory role, diffusing through the extracellular environment to affect various cell types, consistent with its extrasynaptic release and the widespread distribution of dopamine receptors (Veruki and Wässle, 1996; Nguyen-Legros et al., 1999; Puopolo et al., 2001). Dopamine is thought to play a role in mediating light adaptation and in the transition between scotopic and photopic vision by regulating gap-junctional coupling in both the inner and outer retina, consistent with a neuromodulatory role (Xin and Bloomfield, 1999; Weiler et al., 2000). The relative lack of regularity among the DA cells, therefore, may not impede their functional role, to be contrasted with the precise spatiotemporal transfer of visual information associated with other retinal neurons and their targets.

Tangential dispersion is insufficient to account for the exclusion zone

In other regularly distributed populations of retinal nerve cells in the mouse retina, their constituents disperse tangentially (up to 150 μm) at the time of their differentiation (Reese et al., 1999). This dispersion has been suggested to be the biological embodiment of the exclusion zone, reflecting a mutual repulsion between like-type cells that are positioned too close to one another (Eglen et al., 2000, 2003). Since DA cells do not exhibit such universal tangential dispersion during development (Reese et al., 1999), with only a minority (<20%) showing evidence of tangential dispersion, shown here to disperse for distances rarely much greater than one cell diameter, this movement is unlikely to establish the exclusion zones suggested in the above experimental and modeling studies. Furthermore, our attempt to simulate this degree of movement within a population of randomly distributed cells, in which those that are nearest one another are moved apart, was found to increase regularity only marginally, well short of the indexes we observed in the real data. Finally, the *bcl-2* data suggest that close proximity may not drive tangential dispersion in the DA cells, since these retinas contained cells that were adjacent to one another as frequently as random simulations would predict. Together, these results suggest that some other explanation should account for the presence of the exclusion zone surrounding DA cells.

Lateral inhibitory fate-determining events do not underlie the exclusion zone

One suggestion is that lateral inhibition by newborn DA cells might prohibit neighboring cells from adopting a similar fate during development, as has been shown in the developing frog retina (Reh and Tully, 1986). Such a mechanism would ensure that no two DA cells are ever closer to one another than some minimal distance. This mechanism could in principle account for the exclusion zones observed in the normal mouse retina, although some other explanation would still be required to explain the apparent lack of patterning among those DA cells. One possible explanation for that latter effect is that cell death leads to the elimination of a subset of an initially regular mosaic having a periodicity associated with the minimal distance spacing rules outlined here. According to this hypothesis, lateral inhibitory events at the time of dopaminergic cell fate determination prevent neighboring cells from adopting the same fate; such fate-determining events occurring repeatedly across the retina then establish a patterning which is subsequently degraded by cell death. The present analysis of *bcl-2* overexpressing retinas refutes this account as the cause of the exclusion zone, since these *bcl-2* overexpressing retinas contain frequent pairs of DA cells, indicating that neighboring cells can acquire the same fate. In fact, these cells occur side-by-side in the *bcl-2* overexpressing retinas as often as a random simulation would predict. Furthermore, their mosaic regularity is worse, not better, than that found in the depleted wildtype retina. These results then weigh against a feedback-inhibitory fate deterministic account of the exclusion zone underlying the mosaic of DA cells in the normal retina. We cannot, however, rule out other fate-deterministic accounts; for example, that the excessive ganglion cell population in these *bcl-2*-overexpressing retinas has modified the pattern of potential inductive signals that define the dopaminergic amacrine cell fate.

Cell death sculpts the exclusion zone

Alternatively, DA cells may compete locally for some target- or afferent-derived trophic substance during normal development (Linden et al., 1998), such that close proximity to a neighboring cell may reduce the likelihood of acquiring adequate sustaining factor, in turn causing that cell to undergo apoptosis. Consistent with this, early BDNF treatment has been shown to increase the number of DA cells while BDNF-knockout mice contain fewer DA cells (Cellerino et al., 1998), and BDNF-trkB signaling modulates the frequency of cell death within the amacrine cell layer (Cusato et al., 2002). Retinal ganglion cells could be one such source of BDNF (Cohen-Cory and Fraser, 1994; Perez and Caminos, 1995; Cohen-Cory et al., 1996; Das et al., 1997), and these *bcl-2* overexpressing mice have a larger than normal number of retinal ganglion cells (Cenni et al., 1996). Early elimination of the retinal ganglion cells might therefore be expected to reduce the number of DA cells, yet in the ferret retina it does not do so (Williams et al., 2001). Whatever the determinants of this DA cell death, its regulation may produce the exclusion zones that we have detected in maturity (Eglen and Willshaw, 2002).

Other populations of retinal neurons undergo naturally occurring cell death, yet this cell death does not always improve mosaic regularity. Cholinergic amacrine cells in the INL of the mouse retina, for example, undergo a 20% reduction in numbers between P-4 and P-12, yet their mosaic regularity does not change during this period (Galli-Resta and Novelli, 2000), and manipulations that rescue alpha retinal ganglion cells in the cat's retina from naturally occurring cell death do not produce a less regular mosaic (Kirby and Chalupa, 1986). That very cell class, however, has been shown to be less regular before naturally occurring cell death (Jeyarasasingam et al., 1998), suggesting that some other dynamic mechanism must be responsible for establishing regularity following such rescue; for instance, cell–cell interactions that drive tangential dispersion (Reese et al., 1995). The present investigation was not able to chart the developmental time-course of the dopaminergic amacrine cells because these cells express tyrosine hydroxylase only relatively late, after the period of naturally occurring cell death. To the extent that the *bcl-2* overexpressing retina reveals a spatial arrangement present in wildtype mice during normal develop-

ment, one would like to understand the determinants of DA cell fate and how it is regulated in a spatially random manner. But with respect to the present concerns, these results suggest that the death of DA cells, by virtue of their proximity to others that survive, transforms an initially random distribution into a more regular one. Whatever the means by which proximity might lead to cell death, this mechanism does not appear to be regulated on a precise spatial scale, particularly since a death rate of 90% based strictly on proximity should produce a far more regular mosaic than that achieved here (Eglen and Willshaw, 2002). Presumably, temporal as well as spatial constraints influence the extent to which proximity controls survival, sculpting the marginally regular dopaminergic mosaics shown here. These results, in conjunction with previous studies, show that multiple biological mechanisms may ultimately underlie the manifestation of exclusion zones in the developing retina that serve to space cells apart from one another.

ACKNOWLEDGMENTS

LITERATURE CITED

Ammermüller J, Möckel W, Rugan P. 1993. A geometrical description of horizontal cell networks in the turtle retina. Brain Res 616:351–356.

Cellerino A, Pinzon-Duarte G, Carroll P, Kohler K. 1998. Brain-derived neurotrophic factor modulates the development of the dopaminergic network in the rodent retina. J Neurosci 18:3351–3362.

Cenni MC, Bonfanti L, Martinou JC, Ratto GM, Strettoi E, Maffei L. 1996. Long-term survival of retinal ganglion cells following optic nerve section in adult bcl-2 transgenic mice. Eur J Neurosci 8:1735–1745.

Cohen-Cory S, Fraser SE. 1994. BDNF in the development of the visual system of Xenopus. Neuron 12:747–761.

Cohen-Cory S, Escandon E, Fraser SE. 1996. The cellular patterns of BDNF and *trkB* expression suggest multiple roles for BDNF during *Xenopus* visual system development. Dev Biol 179:102–115.

Cook JE. 1996. Spatial properties of retinal mosaics: an empirical evaluation of some existing measures. Vis Neurosci 13:15–30.

Cook JE, Chalupa LM. 2000. Retinal mosaics: new insights into an old concept. TINS 23:26–34.

Cusato K, Bosco A, Linden R, Reese BE. 2002. Cell death in the inner nuclear layer of the retina is modulated by BDNF. Dev Brain Res 139:325–330.

Dacey DM. 1990. The dopaminergic amacrine cell. J Comp Neurol 301:461–489.

Das I, Hempstead BL, Macleish PR, Sparrow JR. 1997. Immunohistochemical analysis of the neurotrophins BDNF and NT-3 and their receptors trk B, trk C, and p75 in the developing chick retina. Vis Neurosci 14:835–842.

Diggle PJ. 1979. On parameter estimation and goodness-of-fit testing for spatial point patterns. Biometrics 35:87–101.

Diggle PJ. 1983. Statistical analysis of spatial point patterns. London: Academic Press.

Eglen SJ, Willshaw DJ. 2002. Influence of cell fate mechanisms upon retinal mosaic formation: a modelling study. Development 129:5399–5408.

Eglen SJ, van Ooyen A, Willshaw DJ. 2000. Lateral cell movement driven by dendritic interactions is sufficient to form retinal mosaics. Network: Comput Neural Syst 11:103–118.

Eglen SJ, Galli-Resta L, Reese BE. 2003. Theoretical models of retinal mosaic formation. In: van Ooyen A, editor. Modelling Neural Development. Boston: MIT Press.

Galli-Resta L, Novelli E. 2000. The effects of natural cell loss on the regularity of the retinal cholinergic arrays. J Neurosci 20:RC60(1–5).

Galli-Resta L, Resta G, Tan S-S, Reese BE. 1997. Mosaics of islet-1 expressing amacrine cells assembled by short range cellular interactions. J Neurosci 17:7831–7838.

Galli-Resta L, Novelli E, Kryger Z, Jacobs GH, Reese BE. 1999. Modelling the mosaic organization of rod and cone photoreceptors with a minimal-spacing rule. Eur J Neurosci 11:1461–1469.

Galli-Resta L, Novelli E, Viegi A. 2002. Dynamic microtubule-dependent interactions position homotypic neurones in regular monolayered arrays during retinal development. Development 129:3803–3814.

Gustincich S, Feigenspan A, Wu DK, Koopman LJ, Raviola E. 1997. Control of dopaminergic release in the retina: a transgenic approach to neural networks. Neuron 18:723–736.

Jeyarasasingam G, Snider CJ, Ratto G-M, Chalupa LM. 1998. Activity-regulated cell death contributes to the formation of ON and OFF alpha ganglion cell mosaics. J Comp Neurol 394:335–343.

Kirby M, Chalupa LM. 1986. Retinal crowding alters the morphology of alpha ganglion cells. J Comp Neurol 251:532–541.

Kolb H, Nelson R, Mariani A. 1981. Amacrine cells, bipolar cells and ganglion cells of the cat retina. Vision Res 21:1081–1114.

Linden R, Rehen SK, Chiarini LB. 1998. Apoptosis in developing retinal tissue. Prog Ret Eye Res 18:133–165.

Mariani AP, Hokoc JN. 1988. Two types of tyrosine hydroxylase-immunoreactive amacrine cell in the rhesus monkey retina. J Comp Neurol 276:81–91.

Martin-Martinelli E, Savy C, Nguyen-Legros J. 1994. Morphometry and distribution of displaced dopaminergic cells in rat retina. Brain Res Bull 34:467–482.

McCabe KL, Gunther EC, Reh TA. 1999. The development of the pattern of retinal ganglion cells in the chick retina: mechanisms that control differentiation. Development 126:5713–5724.

Müller B, Peichl L. 1991. Morphology and distribution of catecholaminergic amacrine cells in the cone-dominated tree shrew retina. J Comp Neurol 308:91–102.

Nguyen-Legros J. 1988. Morphology and distribution of catecholamine-neurons in mammalian retina. Prog Ret Res 7:113–147.

Nguyen-Legros J, Versaux-Botteri C, Vernier P. 1999. Dopamine receptor localization in the mammalian retina. Mol Neurobiol 19:181–204.

Oyster CW, Takahashi ES, Cillufo M, Brecha N. 1985. Morphology and distribution of tyrosine hydroxylase-like immunoreactive neurons in the cat retina. Proc Natl Acad Sci USA 82:6445–6339.

Peichl L. 1991. Catecholaminergic amacrine cells in the dog and wolf retina. Vis Neurosci 7:575–587.

Perez MTR, Caminos E. 1995. Expression of brain-derived neurotrophic factor and of its functional receptor in neonatal and adult retina. Neurosci Lett 183:96–99.

Puopolo M, Hochstetler SE, Gustincich S, Wightman RM, Raviola E. 2001. Extrasynaptic release of dopamine in a retinal neuron: activity dependence and transmitter modulation. Neuron 30:211–225.

Raven MA, Reese BE. 2002. Horizontal cell density and mosaic regularity in pigmented and albino mouse retina. J Comp Neurol 454:168–176.

Reese BE, Galli-Resta L. 2002. The role of tangential dispersion in retinal mosaic formation. Prog Ret Eye Res 21:153–168.

Reese BE, Tan S-S. 1998. Clonal boundary analysis in the developing retina using X-inactivation transgenic mosaic mice. Sem Cell Dev Biol 9:285–292.

Reese BE, Harvey AR, Tan S-S. 1995. Radial and tangential dispersion patterns in the mouse retina are cell-class specific. Proc Natl Acad Sci USA 92:2494–2498.

Reese BE, Necessary BD, Tam PPL, Faulkner-Jones B, Tan S-S. 1999. Clonal expansion and cell dispersion in the developing mouse retina. Eur J Neurosci 11:2965–2978.

Reh TA, Tully T. 1986. Regulation of tyrosine hydroxylase-containing amacrine cell number in larval frog retina. Dev Biol 114:463–469.

Ripley BD. 1976. The second-order analysis of stationary point processes. J Appl Probab 13:255–266.

Rodieck RW. 1991. The density recovery profile: A method for the analysis of points in the plane applicable to retinal studies. Vis Neurosci 6:95–111.

Savy C, Yelnik J, Martin-Martinelli E, Karpouzas I, Nguyen-Legros J. 1989. Distribution and spatial geometry of dopamine interplexiform cells in the rat retina. I. Developing retina. J Comp Neurol 289:99–110.

Shapiro MB, Schein SJ, deMonasterio FM. 1985. Regularity and structure of the spatial pattern of blue cones of macaque retina. J Am Stat Assoc 80:803–814.

Strettoi E, Volpini M. 2002. Retinal organization in the bcl-2-overexpressing transgenic mouse. J Comp Neurol 446:1–10.

Tauchi M, Madigan NK, Masland RH. 1990. Shapes and distributions of the catecholamine-accumulating neurons in the rabbit retina. J Comp Neurol 293:178–189.

Versaux-Botteri C, Nguyen-Legros J, Vigny A, Raoux N. 1984. Morphology, density and distribution of tyrosine hydroxylase-like immunoreactive cells in the retina of mice. Brain Res 301:192–197.

Veruki ML, Wässle H. 1996. Immunohistochemical localization of dopamine D_1 receptors in rat retina. Eur J Neurosci 8:2286–2297.

Wässle H, Riemann HJ. 1978. The mosaic of nerve cells in the mammalian retina. Proc R Soc (Lond) B 200:441–461.

Weiler R, Pottek M, He S, Vaney DI. 2000. Modulation of coupling between retinal horizontal cells by retinoic acid and endogenous dopamine. Brain Res Rev 32:121–129.

Wikler KC, Rakic P. 1994. An array of early differentiating cones precedes the emergence of the photoreceptor mosaic in the fetal monkey retina. Proc Natl Acad Sci USA 91:6534–6538.

Williams RR, Cusato K, Raven M, Reese BE. 2001. Organization of the inner retina following early elimination of the retinal ganglion cell population: effects on cell numbers and stratification patterns. Vis Neurosci 18:233–244.

Wulle I, Schnitzer J. 1989. Distribution and morphology of tyrosine hydroxylase-immunoreactive neurons in the developing mouse retina. Dev Brain Res 48:59–72.

Xin D, Bloomfield SA. 1999. Dark- and light-induced changes in coupling between horizontal cells in mammalian retina. J Comp Neurol 405:75–87.